Contributions of the RNA-Binding and Linker Domains and RNA Structure to the Specificity and Affinity of the Nucleolin RBD12/NRE Interaction†

L. David Finger,‡ Carina Johansson,‡ Bruno Rinaldi,§ Philippe Bouvet,§ and Juli Feigon*,‡

Department of Chemistry and Biochemistry, and Molecular Biology Institute, University of California, Los Angeles, California 90095-1569, and Ecole Normale Supérieure de Lyon, UMR CNRS 5665, 46 alleé d'italie, 69364 Lyon, Cedex 07, France

Received January 12, 2004; Revised Manuscript Received March 29, 2004

ABSTRACT: Nucleolin is a multidomain phosphoprotein involved in ribosome biogenesis. In vitro selection and binding studies with pre-rRNA fragments have shown that the first two RNA-binding domains (RBDs) in nucleolin (RBD12) recognize the consensus sequence (U/G)CCCG(A/G) in the context of a stem-loop structure (nucleolin-recognition element = NRE). Structural studies of nucleolin RBD12 in complex with an in vitro selected NRE (sNRE) and a natural pre-rRNA NRE (b2NRE) have revealed that sequence-specific binding of the consensus NRE is achieved in a similar manner in both complexes using residues in both RBDs as well as the linker connecting them. Using fluorescence anisotropy (FA) and nuclear magnetic resonance (NMR), we demonstrate the importance of the linker for NRE affinity by showing that only the individual RBDs with the linker attached retain the ability to specifically bind, albeit weakly, to sNRE and b2NRE. Binding of RBD1 and RBD2 to the NREs in trans is not detected even when one of the RBDs has the linker attached, which suggests that the linker also contributes to the affinity by tethering the two RBDs. To determine if binding of nucleolin RBD12 to natural NREs is dependent on a specific RNA stem-loop structure, as was the case for the sNRE, we conducted FA and NMR binding assays with nucleolin RBD12 and a single-stranded NRE. The results show that nucleolin RBD12 sequence-specifically binds a single-stranded NRE with an affinity similar to that for b2NRE, indicating that a stem-loop structure is not required for the nucleolin RBD12/pre-rRNA NRE interaction.

The RNA-binding domain (RBD),[1] also known as the RNA-recognition motif (RRM), is the third most common protein motif found in nature (*1*, *2*). Proteins containing RBDs have been shown to participate in many essential cellular processes in RNA metabolism including pre-mRNA splicing, mRNA stability, RNA packaging and transport (*1*), and rRNA processing (*3*, *4*). Nuclear magnetic resonance (NMR) and crystallographic studies have shown that the RBDs, which are comprised of 70−100 amino acids, have a characteristic $\beta\alpha\beta\beta\alpha\beta$ fold with the two α helices packing against a four-stranded antiparallel β sheet (*5*, *6*). The central two β strands have conserved octameric RNP-1 and hexameric RNP-2 motifs, which contain aromatic, hydrophobic, and basic amino acids (*7*) that are used to sequence-specifically bind single-stranded RNA, stem-loop RNA structures (*6*), and sometimes DNA (*8*). Many RNA-binding proteins contain multiple RBDs separated by linkers of variable amino acid composition and length (*9*). In the case of the snRNP U1A protein, which has two RBDs, a single RBD accounts for the affinity for the RNA target (*10*−*12*). In contrast, the multiple RBD proteins poly(A)-binding protein (PABP) (*13*), sex-lethal protein (Slx) (*14*, *15*), ASF/SF2 (*16*, *17*), hnRNP A1 (*18*, *19*), HuC (*20*), HuD (*21*, *22*), and nucleolin (*3*, *23*) require the simultaneous binding of more than one RBD for optimal binding of a target RNA sequence.

Nucleolin, which contains four tandem RBDs, is the most abundant protein in the nucleoli of vertebrate cells and is thought to participate in several steps of ribosome biogenesis, including regulation of rDNA transcription, rRNA processing, ribosome assembly, and nucleocytoplasmic transport (Figure 1A) (*3*, *24*). Nucleolin associates directly with nascent pre-rRNA but is not found in cytoplasmic ribosomes (*25*). Attempts to understand the multiple roles of nucleolin in ribosome biogenesis have involved characterization of the pre-rRNA sequences recognized by the RBDs, because the functions of nucleolin are likely reflected in its RNA-binding properties. In vitro selection in combination with mutagenesis

† This work was supported by NIH Grant R01 GM37254 to J.F. and an ATIP from the CNRS, the Région Rhone-Alpes, and the Ministère de la Recherche (AC nanosciences) to P.B.

* To whom correspondence should be addressed. E-mail: feigon@mbi.ucla.edu. Phone: (310) 206-6922. Fax: (310) 825-0982.

‡ University of California, Los Angeles.

§ Ecole Normale Supérieure de Lyon.

[1] Abbreviations: RBD, RNA-binding domain; RRM, RNA-recognition motif; NRE, nucleolin-recognition element; RNP-1, octameric repeat found in RBD; RNP-2, hexameric repeat found in RBD; PABP, poly(A)-binding protein; Slx, sex-lethal protein; sNRE, in vitro selected NRE; b2NRE, natural NRE found in the mouse 5′ external transcribed spacer (nts: 562 to 578 EMBL sequence database accession code M20154); RBD1, first RBD in Chinese hamster nucleolin (residues: V298−P381); RBD2, second RBD in Chinese hamster nucleolin (residues: T394−G469); RBD12, RBD1 and RBD2; linker, 12 amino acid residues in Chinese hamster nucleolin tethering RBD1 and RBD2 (residues: K382−R393); RBD1L, protein construct of RBD1 including the linker residues at C terminus of RBD1; LRBD2, protein construct of RBD2 including the linker residues at the N terminus of RBD2; NMR, nuclear magnetic resonance; FA, fluorescence anisotropy; HSQC, heteronuclear single-quantum coherence; K_D, dissociation constant.

10.1021/bi049904d CCC: $27.50
Published on Web 05/13/2004

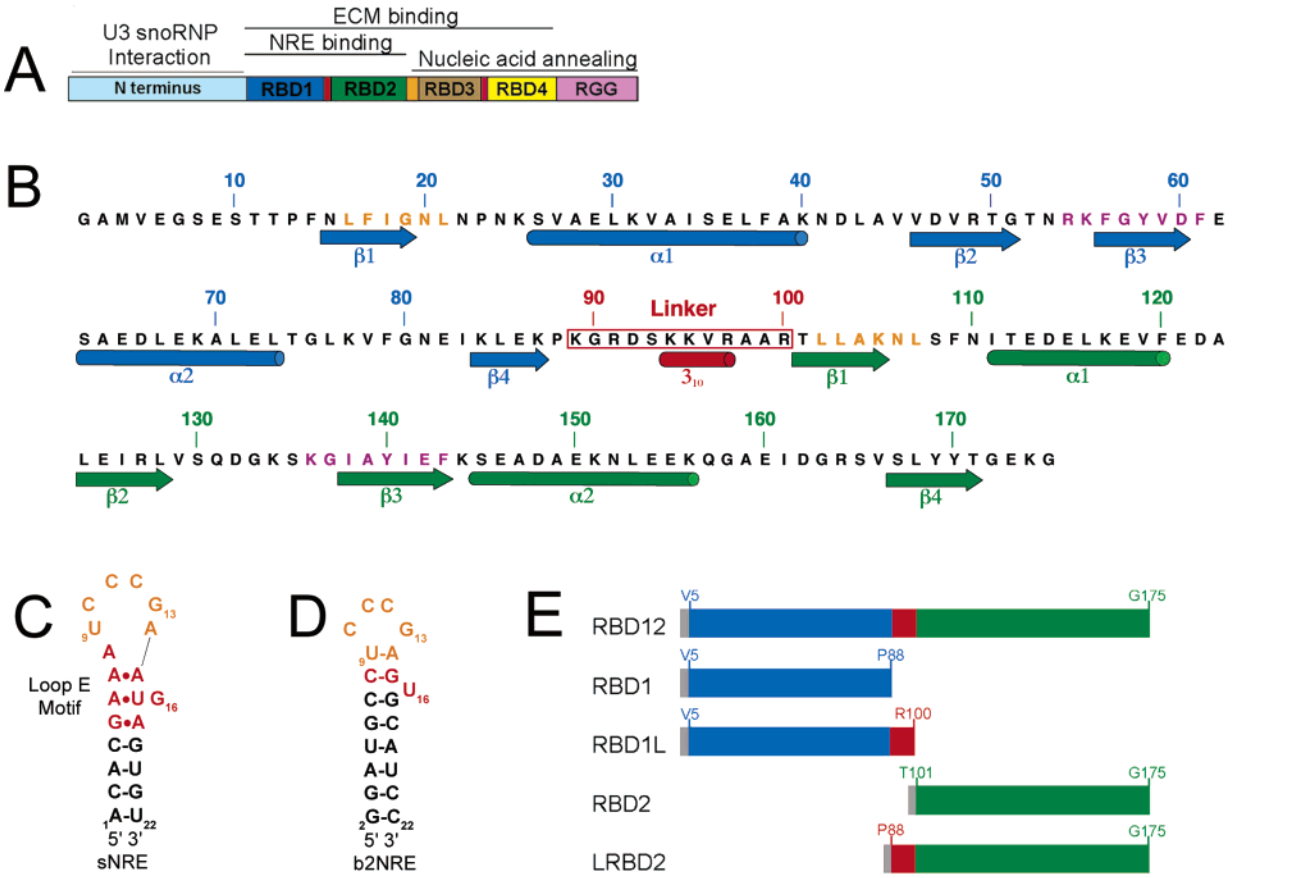

FIGURE 1: (A) Domain organization of hamster nucleolin. Some of the known functions of the nucleolin domains are indicated above. The N terminus is known to interact with U3 snoRNP (*58*), RBD12 binds the NRE (*28*), RBD1234 binds the ECM (*23*), and RBD34RGG has been shown to have nucleic acid annealing activity (*59*). (B) Amino acid sequence of hamster nucleolin RBD12 used in this paper (SWISS−PROT accession code P08199). Secondary structure elements determined for hamster nucleolin RBD12 are indicated below the sequence and are shown in blue for RBD1, red for the linker, and green for RBD2. The hexameric RNP-2 and octameric RNP-1 motifs are highlighted in orange and purple, respectively. The linker residues are shown in a red box. V5−G175 corresponds to amino acid residues 298−468 in the full protein. The first three amino acids at the N terminus are left after TEV cleavage of the 20 amino acid residue $(His)_6$ purification tag. (C) Secondary structure of the sNRE used in this paper (*29*). Nucleotides 3−20 are the sequence identified by in vitro selection (*25*). The NRE consensus is shown in orange, additional loop nucleotides shown in red, and the stem shown in black. Two G•C base pairs, which are at the end of the stem for the purpose of transcription, are not shown. (D) Secondary structure representation of b2NRE used in this paper. Nucleotides 4−20 correspond to the B2 sequence found in mouse pre-RNA (nts 562−578; EMBL sequence database accession code M20154). The color scheme is the same as in C. The sequences of (C) sNRE and (D) b2NRE are numbered to correspond to the original sNRE construct (*30*, *36*). (E) Schematic representation of the RBD12 subdomains used in this paper, with the color scheme for the domains being the same as in B. The gray box at each N terminus represents the three amino acids residues left after TEV cleavage of the affinity tag.

and structural analysis has identified sequences in pre-rRNA to which nucleolin can bind specifically (*23*, *26*). One family of RNA sequences that nucleolin binds is called the nucleolin-recognition element (NRE), which is defined as a RNA containing the consensus (U/G)CCCG(A/G) in a loop of variable size (7−14 nucleotides) and at least a four base-pair stem (*25*). Two of the 39 putative mouse NREs, B1 (nts 515−532) and B2 (nts 562−578), located in the 5′-ETS region of mouse pre-rRNA (EMBL sequence database accession code M20154), have been confirmed as nucleolin-binding sites by cross-linking studies (*27*). Subsequent studies have shown that the interaction of nucleolin with an in vitro selected NRE only requires the first two RBDs of nucleolin (Figure 1B) in a cis arrangement for nanomolar affinity (K_D = 1−5 nM) (*28*). More recently, constructs of B1 and B2 NREs, b1NRE and b2NRE, respectively, have been shown to also bind with nanomolar affinity to nucleolin RBD12, albeit approximately 100−500-fold more weakly than the in vitro selected NRE (sNRE) (*29*).

We previously determined the solution structure of nucleolin RBD12 in complex with a 22 nucleotide RNA stem loop containing the 18 nucleotide in vitro selected consensus sequence (sNRE) (Figure 1C) (PDB accession code 1FJE) (*30*) and more recently with the 21 nucleotide b2NRE stem loop (Figure 1D) (PDB accession code 1RKJ) (*31*). Both structures show that the specificity for the NRE consensus sequence is determined by intermolecular stacking and hydrogen-bond interactions involving amino acids on the β-sheet surface of the RBDs and in the linker and loops as well. The linker connecting the two RBDs plays an important role in both complexes by making specific and nonspecific contacts to the NRE consensus sequence. Furthermore, the upper part of the sNRE stem, which is not part of the NRE consensus sequence, folds into a loop E motif (S turn) (*32*−*35*). In the RBD12/sNRE complex, nucleotides in the upper part of the loop E motif and the nonconsensus A8, which is stacked on top of the loop E motif, are also specifically recognized by amino acid residues in RBD1 and the linker

(*30*, *36*). In contrast, the intermolecular interactions in the nucleolin RBD12/b2NRE complex are restricted to the NRE consensus sequence. Kinetic and gel shift analyses have shown that the presence of additional contacts to nonconsensus nucleotides is responsible for the increased stability of the nucleolin RBD12/sNRE complex compared to the nucleolin RBD12/b2NRE complex. In addition, the gel shift analysis showed that the additional contacts to nonconsensus nucleotides in the sNRE are not only nucleotide-specific, but also dependent on the RNA secondary structure (i.e., formation of the loop E motif at the top of the stem) (*31*). In summary, these studies illustrate the importance of the RNA secondary structure in the nucleolin RBD12/sNRE interaction and provide a rationale for the stem-loop requirement of the sNRE.

Prior to structure determination of the nucleolin RBD12/sNRE complex, the 12 amino acid residue linker connecting the two RBDs was only thought to restrict the positions of the RBDs relative to one another and promote the association of the two RBDs with the same RNA (*37*). However, the structures of the nucleolin RBD12/sNRE and RBD12/b2NRE complexes and gel-shift assays with RBD12 constructs containing linker mutations demonstrated the importance of the linker for the nucleolin RBD12/NRE interaction (*30*). Most analyses of sequence-specific binding and affinity of RNA-binding proteins containing multiple RBDs have focused on the role of the RBDs. Here, NMR and fluorescence anisotropy (FA) studies of the interaction of RBD1 and RBD2 protein constructs with and without the linker are used to demonstrate the importance of the linker for the affinity, specificity, and domain cooperativity of the nucleolin RBD12/NRE interaction. The structures of other $(RBD)_2$/RNA complexes (*38*−*40*) also show interaction of the linker residues to the target RNA, suggesting that the above results are general. FA assays and NMR were also used to determine if binding of nucleolin RBD12 to a natural pre-rRNA target was dependent on a specific stem-loop structure, as was the case for the sNRE. Our results show that nucleolin RBD12 can sequence-specifically bind a single-stranded NRE with a K_D similar to that observed for b2NRE. We have previously proposed that the nucleolin/NRE interaction is important for proper folding of nascent pre-rRNA (*30*). The fact that nucleolin RBD12 binds single-stranded NREs supports the proposal that nucleolin initially binds single-stranded NRE substrates to facilitate formation of transient stem-loop structures in pre-rRNA.

MATERIALS AND METHODS

RNA Synthesis and Purification. Unlabeled and uniformly ^{13}C,^{15}N-labeled RNA oligonucleotides for NMR studies were prepared by in vitro transcription as described (*41*), except for the single-stranded substrates, which were chemically synthesized (Dharmacon, Boulder, CO) and purified as previously described (*41*). b2NRE and sNRE were annealed at dilute concentrations (1−10 μM) in water and adjusted to the desired salt conditions by the addition of the appropriate stock solution. sNRE buffer consisted of 10 mM potassium phosphate at pH 7, 100 mM KCl, 50 μM ethylenediaminetetraacetic acid (EDTA), and 0.02% NaN_3, and b2NRE buffer consisted of 5 mM potassium phosphate at pH 7, 50 μM EDTA, and 0.02% NaN_3. Single-stranded substrates were diluted in water. All RNAs were subsequently concentrated by ultrafiltration (Amicon).

Constructs. Previous attempts to cleave the affinity tag from the pET15b vector-expressed nucleolin RBD12 using thrombin resulted in cleavage of the linker as well. Therefore, RBD12 and subdomains were cloned into a pProEX HT vector to allow for cleavage of the $(His)_6$ affinity tags from the RBD12 subdomains using TEV protease (*42*) instead of thrombin. The hamster nucleolin RBD12 subdomains were generated by PCR using Vent DNA polymerase and the pet15b vector containing the hamster nucleolin RBD12 gene (*43*). The 5′ oligonucleotide used to amplify RBD12, RBD1, and RBD1L was 5′-CATGCCATGGTGGAAGGTTCAGAATCAACTACAC-3′; the 5′ oligo for RBD2 was 5′-CATGCCATGGCAACACTTTTAGCAAAAAATCTTTC-3′; the 5′ oligo for RBD2L was 5′-ACGGATCCAAAAGGAAGAGATAGTAAAAAAG-3′; the 3′ oligo for RBD12, RBD2, and RBD2L was 5′-GCGAAGCTTCATCCCTTCTCCCCAGTATAGTAAAG-3′; the 3′ oligo for RBD1 was 5′-ACCAAGCTTCATGGTTTTTCTAGTTTAATTTCATTGCC-3′; and the 3′ oligo for RBD1L was 5′-ACCAAGCTTCACCTTGCAGCTCGAACTTTTTTACTATC-3′. After amplification, PCR fragments were subcloned into pProEX HT using the restriction sites *Nco* I−*Hin*d III for RBD12, RBD1, RBD1L, and RBD2 and *Bam*H I−*Hin*d III for RBD2L.

Protein Expression and Purification. BL21-Codon Plus-RIL (Stratagene) cells were transformed with recombinant pProEX HT (Life Technologies) plasmids containing an insert encoding for the hamster nucleolin $(His)_6$-RBDX subdomains, where RBDX stands for RBD12, RBD1, RBD1L, RBD2, and LRBD2. Cells grown at 37 °C in LB media containing 100 μg/mL ampicillin and 35 μg/mL chloramphenicol were induced with 1 mM isopropyl-1-thio-β-D-galactopyranoside at $OD_{600} = 0.6-0.8$ and grown for an additional 3 h. Harvested cells were resuspended in 20 mM sodium phosphate at pH 7.4, 500 mM NaCl with 0.1% Triton X-100, and 100 μL of protease cocktail inhibitor (Sigma) per liter of culture, and lysed by three freeze−thaw cycles and sonication. Proteins were then purified as previously described (*29*), except that the cleavage of the $(His)_6$ tag was accomplished with $(His)_6$-TEV S219N protease (*42*).

FA Assays. 5′-fluorescein-labeled RNAs with sequences corresponding to those shown in Figure 1 were obtained from Dharmacon Research, purified, deprotected, and desalted. 5′-fluoroscein-NRE substrates were diluted in TE buffer (10 mM Tris-HCl at pH 8.0 and 1 mM EDTA) and quantified at A_{260} as described (*44*). FA was measured using the Beacon 2000 Variable Temperature Fluorescence Polarization System (Panvera, Madison, WI) with fixed excitation (490 nM) and emission (535 nM). Equilibrium binding assays were performed as previously described (*29*). Polarization values were converted to anisotropy values using eq 1. Data are expressed

$$A = \frac{2P}{3 - P} \tag{1}$$

as $(A - A_0)/A_0$, where A is the anisotropy of the fluorescein-labeled RNA at the indicated amount of protein and A_0 is the anisotropy for the free-labeled RNA or mA, where the mA is 1000 times the anisotropy of the fluorescein-labeled RNA at the indicated amount of protein. Dissociation

constants (K_D's) were calculated by fitting data to eq 2 using KaleidaGraph.

$$A = A_{\mathrm{RNA_F}} + (A(\mathrm{P-RNA}) - A_{\mathrm{RNA_F}}) \left\{ \frac{[\mathrm{RNA}]_T + K_D + [\mathrm{P}]_T - \sqrt{(-[\mathrm{RNA}]_T - K_D - [\mathrm{P}]_T)^2 - 4[\mathrm{RNA}]_T[\mathrm{P}]_T}}{2[\mathrm{RNA}]_T} \right\} \quad (2)$$

NMR Spectroscopy. All NMR spectra were recorded on Bruker DRX 500 or 600 MHz spectrometers. Protein−RNA complexes were prepared by addition of aliquots of lyophilized RNA or protein until the indicated molar ratio was achieved. Titration of nucleolin RBD12 and RBD12 subdomains into 0.15 mM ^{13}C,^{15}N-labeled sNRE or b2NRE was monitored at 310 K by gradient sensitivity enhanced ^1H-^{13}C heteronuclear single-quantum coherences (HSQCs) (*45*). Titration of SSNRE or SSNS into 0.15 mM ^{15}N-labeled nucleolin RBD12 was monitored at 310 K by ^1H-^{15}N HSQCs with WATERGATE (*46*) water suppression. Spectra were processed and analyzed using Bruker XWINNMR 2.6 and Felix97 (MSI, Inc.).

RESULTS

Determination of Dissociation Constants of the Individual RBDs and NREs. Many proteins that bind RNA contain multiple RBDs, and two or more tandem RBDs are often necessary for high-affinity binding to RNA targets (*9*). Although most analyses of sequence-specific recognition in $(RBD)_2$/RNA complexes have focused on the role of the RBDs, several crystal and NMR structures of $(RBD)_2$/RNA complexes show that the linker residues connecting the two RBDs also contribute to RNA binding (*30*, *38*−*40*). For instance, in the nucleolin RBD12/sNRE and RBD12/b2NRE complexes, the linker residues connecting RBD1 and RBD2 interact with the NREs in both sequence- and nonsequence-specific manners. In light of these observations, we decided to further investigate the role of the linker in nucleolin RBD12/NRE binding by assaying for individual binding of isolated RBD1 and RBD2 with and without the linker attached. The RBD12 subdomains that were used in this paper are shown in Figure 1E. Because the presence of the 20 amino acid residue N-terminal $(His)_6$ tag used in purification could interfere with LRBD2, RBD2, and trans binding, cleavage of the affinity tag from all constructs was necessary. TEV protease treatment resulted in RBD12 subdomains of the expected size (data not shown).

Use of the EMSA procedure previously shown to result in band shifts for the nucleolin RBD12/sNRE and RBD12/b2NRE complexes (*29*) did not result in band shifts for any of the nucleolin RBD12 subdomains with sNRE or b2NRE (data not shown). Because EMSA is a nonequilibrium binding assay, the lack of a band shift does not necessarily indicate the absence of binding, as low-affinity complexes may have dissociated during the course of electrophoresis (*44*). Therefore, FA binding assays were employed because it is an equilibrium binding technique and, thus, does not require the separation of bound and free RNA (*44*). The results of titrations of varying concentrations of RBD1, RBD1L, RBD2, and LRBD2 into 5′-fluorescein-labeled sNRE and b2NRE are shown in Figure 2. Both RBD1L and LRBD2 bind the sNRE and b2NRE hairpins, but no binding to the NREs is observed for the individual domains in the absence of linker residues. Fitting the data for RBD1L and LRBD2 to eq 2 reveals that the dissociation constants (K_D) for the sNRE and b2NRE interaction vary from 400 to 1000 μM (parts A−D of Figure 2). Using the same FA assay procedure, the K_D's of nucleolin RBD12 for sNRE and b2NRE have previously been reported to be 3 and 300 nM, respectively (parts E and F of Figure 2) (*29*). Thus, removal of one of the RBDs from nucleolin RBD12 causes an approximate 100 000- and 1000-fold loss in affinity for sNRE and b2NRE, respectively, indicating that the presence of both RBDs is essential for nanomolar affinity.

We note that the anisotropy for the complexes of the isolated domains with linkers and hairpin NRE substrates is ~10-fold higher than that obtained with RBD12 and hairpin NRE substrates, even though the molecular weight of the complexes of the individual domains is smaller. This is due to the fact that the nucleolin RBD12/NRE complexes are more compact and spherical, while the hairpin RNA complexes with the individual domains and linker are asymmetric, which would give rise to a larger change in anisotropy.

Binding of Individual RBDs to NREs Studied by NMR. To test the specificity of the low-affinity interaction between the individual RBDs with the linker attached and NREs, titrations of RBD1L and LRBD2 to ^{13}C,^{15}N-labeled sNRE and b2NRE were monitored by ^1H-^{13}C HSQCs. Titration of nucleolin RBD12, RBD1L, or LRBD2 into sNRE causes chemical-shift perturbations only for nucleotides in the loop and at the top of the loop E motif but leaves stem resonances (e.g., C2) mostly unaffected, except for changes in line widths that are consistent with an increased correlation time upon binding of the individual domains (Figure 3). Comparison of parts A and C of Figure 3 shows that the nucleotides that are bound by RBD1 and the linker in the full nucleolin RBD12/sNRE complex (*43*) are also bound by RBD1L, because as the concentration of RBD1L is increased, the chemical shifts of C11, C12, G13, A14, and G16 change to values close to those seen in the nucleolin RBD12/sNRE complex (Figure 3B). C10 is not perturbed upon addition of RBD1L, consistent with the lack of contacts between C10 and RBD1 or the linker. However, U9 is affected by RBD1L addition even though neither RBD1 nor the linker contact U9 in the full nucleolin RBD12/sNRE complex. Perturbation of U9 may be caused indirectly by the interaction between RBD1L and nucleotides A8 and A14, which form an adenine zipperlike motif in the nucleolin RBD12/sNRE complex. When LRBD2 is titrated into sNRE, the nucleotides that are contacted by RBD2 and the linker residues in the full complex are perturbed (e.g., U9, C10, C11, C12, G13, and A14), whereas G16, which is neither close to the binding site nor contacted by RBD2 or the linker, is not affected (parts A and D of Figure 3). Similar results were obtained for titrations of RBD1L and LRBD2 into b2NRE. The chemical-shift changes that are observed upon the addition of RBD1L and LRBD2 to b2NRE are also consistent with the contacts that are made by the individual domains in the nucleolin RBD12/b2NRE complex (*31*) (data not shown). No chemical-shift perturbation of sNRE and b2NRE consensus loop nucleotide resonances is observed when the RBDs lacking the linker residues are titrated into the RNA, an observation that is consistent with the FA

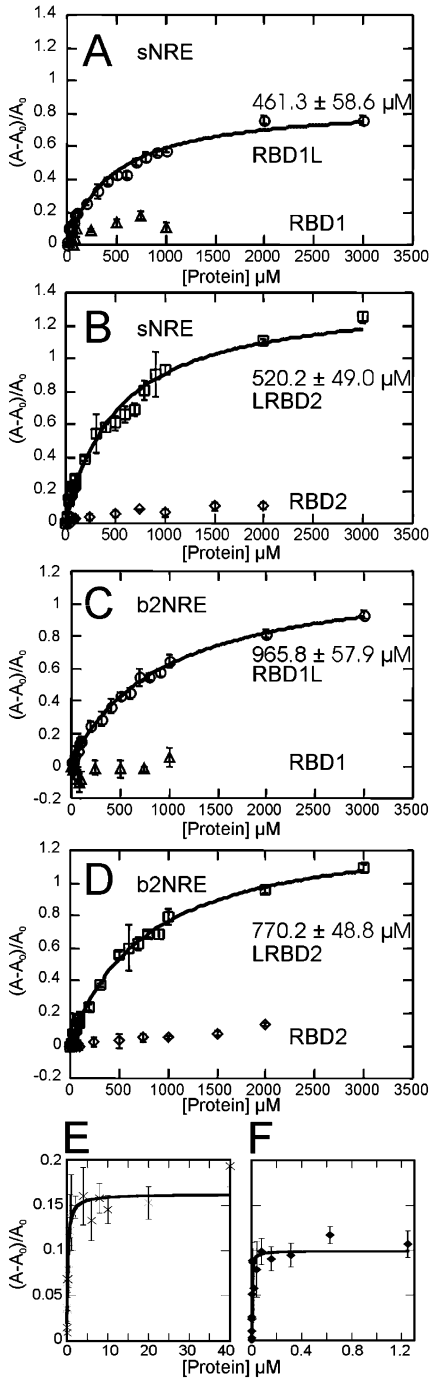

FIGURE 2: Binding isotherms of RBD1/RBD1L (A and C) and RBD2/LRBD2 (B and D), with sNRE (A and B) and b2NRE (C and D) showing that attachment of the linker to either RBD1 or RBD2 results in detectable NRE binding. Binding isotherms were generated with 2 nM sNRE or b2NRE and varying concentrations of RBD1L (○), RBD1 (△), LRBD2 (○), or RBD2 (◇). Each point is an average of five measurements, and the error bars represent the standard deviation of those measurements. Data for RBD1L (○) and LRBD2 (□) were fit to eq 2. The fitted curves are indicated by the black line and have R^2 values greater than 98%. Dissociation constants (K_D's) for (A) RBD1L/sNRE, (B) LRBD2/sNRE, (C) RBD1L/b2NRE, and (D) LRBD2/b2NRE are shown. The RBD12/sNRE (E) and RBD12/b2NRE (F) binding isotherms are shown here for comparison but are plotted on different scales, because of their lower anisotropy (*y* axis) and stronger affinity (*x* axis), but are in the same format as the isolated RBD−linker data. A different format (logarithmic scale) was used in ref *29*, because saturation could be reached for the RBD12/NRE complexes. The nonlogarithmic scale is used here to show that the binding isotherms for the isolated RBDs with the linker are approaching saturation.

results. Because binding of individual domains is observed when the linker residues are present, FA and NMR were also used to assay for trans binding of RBD1L/RBD2 and RBD1/LRBD2. However, these experiments showed no evidence for binding in trans (data not shown). In summary, these results show that the individual domains with the linker attached bind weakly, but specifically, to the NRE consensus nucleotides in a manner similar to that seen in the nucleolin RBD12/sNRE and RBD12/b2NRE complexes. In addition, this paper shows that the RBDs must be covalently linked for both RBDs to bind to the NREs.

Binding of Nucleolin RBD12 to 5′-CUCCCGAGU-3′, a Single-Stranded NRE. Because the nucleolin RBD12/b2NRE complex structure, unlike the nucleolin RBD12/sNRE complex, shows no interactions between the protein and the b2NRE stem (*31*), the requirement for the NRE consensus to be in a stem-loop structure is not clear. To determine if nucleolin RBD12 can sequence-specifically recognize a single-stranded NRE, amide proton and nitrogen chemical shifts of ^{15}N-labeled RBD12 were monitored as a function of the increasing concentration of a RNA oligonucleotide corresponding to loop nucleotides 8−16 of b2NRE (SSNRE). Amide chemical-shift perturbations were observed for residues in the β sheet of both RBDs and in the linker upon addition of SSNRE (Figure 4A). The residues in nucleolin RBD12 that are perturbed upon SSNRE addition have chemical shifts similar to those observed in the nucleolin RBD12/b2NRE complex and are at or near the binding interface (Figure 5A). One notable exception is Y140, a residue in the RNP-1 motif of RBD2 that was shown to interact with the NRE consensus in the nucleolin RBD12/b2NRE and RBD12/sNRE complexes. Although other residues in the RNP-1 motif of RBD2 like I138 and F143 (Figure 1B) show chemical-shift perturbations, Y140, which shows chemical-shift changes when hairpin NREs such as b2NRE and sNRE are titrated into nucleolin RBD12, does not shift upon the addition of SSNRE (Figure 4A). As a specificity control, an oligonucleotide similar to SSNRE but with mutations in the NRE consensus sequence previously shown to abolish NRE binding in the context of a stem loop (U9G/G13A; SSNS) (*31*) was also titrated into a ^{15}N-labeled RBD12 sample. Only very small chemical-shift perturbations of a few residues in RBD1 and of K89 in the linker were observed, but no changes occurred in the rest of the linker and RBD2 (Figure 4B). The observed chemical-shift perturbations are very small compared to the perturbations caused by the addition of an equal amount of SSNRE (parts A and B of Figure 4), which suggests that the interaction is extremely weak, but the binding does involve some of the residues that interact with the NRE nucleotides in the nucleolin RBD12/b2NRE and RBD12/sNRE complexes. These results show that nucleolin RBD12 can sequence-specifically recognize a SSNRE in a manner similar to that of a NRE hairpin.

Most of the chemical-shift changes that are observed in the ^{1}H-^{15}N HSQC spectra of nucleolin RBD12 upon the addition of either b2NRE or SSNRE are similar; however, chemical-shift differences are observed for certain residues (Figure 5A). Mapping of these chemical-shift differences on the lowest energy structure of the nucleolin RBD12/b2NRE complex shows that some of the largest differences are localized to β2 in RBD2 and K94 (Figure 5B). These

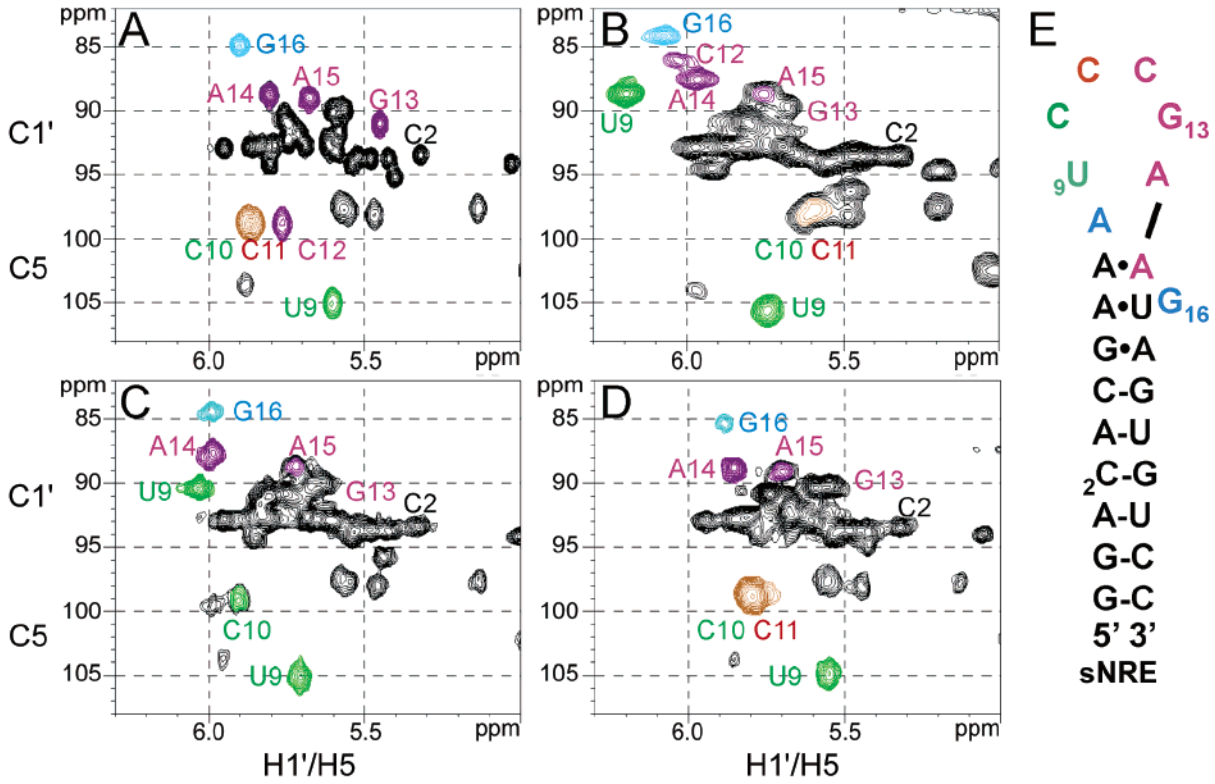

FIGURE 3: RBD1L and LRBD2 sequence specifically bind sNRE. H1′/C1′ and H5/C5 portion of ^{1}H-^{13}C HSQCs of (A) free sNRE, (B) 1:1 nucleolin RBD12/sNRE complex, (C) 2:1 nucleolin RBD1L/sNRE complex, and (D) 2:1 nucleolin LRBD2/sNRE complex. (E) Secondary structure representation and numbering of the sNRE used in the titrations. Nucleotides that are contacted in the nucleolin RBD12/sNRE complex structure (*30*) by RBD1, linker, or RBD2 are shown in blue, red, and green, respectively. Nucleotides contacted by RBD1 and linker (red and blue) are colored purple. Nucleotides not contacted by nucleolin RBD12 are shown in black. Peaks in A−D are labeled and colored the same as in E. Peaks colored brown indicate that a red and green peak are overlapping.

differences are addressed in the Discussion. There are also changes in the exchange kinetics of resonances in nucleolin RBD12 that are perturbed upon addition of SSNRE in comparison to addition of b2NRE. The amide resonances of certain residues located in RBD1 and the linker disappear upon addition of SSNRE and never reappear even when the protein is saturated with the RNA. The disappearance of resonances in RBD1 indicates that binding of RBD1 to SSNRE occurs in the intermediate exchange regime on the NMR time scale at 600 MHz, instead of the slow-exchange regime observed for the nucleolin RBD12/b2NRE titrations at the same field strength. The exchange kinetics are also different for amides in RBD2 and the linker that shift upon addition of SSNRE, from being in the slow-exchange regime in the nucleolin RBD12/b2NRE interaction, to being in the fast-exchange regime in the nucleolin RBD12/SSNRE interaction. To quantify the affinity of the nucleolin RBD12/SSNRE interaction, FA assays using a 5′-fluorescein-labeled SSNRE and varying concentrations of nucleolin RBD12 (Figure 5C) were conducted and show that the K_D's for nucleolin RBD12 binding to b2NRE and SSNRE at 4 °C are within the error of one another (310 ± 110 and 330 ± 54 nM, respectively). The fit of the curve is nonideal at high concentrations of nucleolin RBD12 (>80 μM). Interestingly, this deviation begins in the concentration range in which binding to sNRE and b2NRE was detected for RBD1L and LRBD2 (Figure 2), suggesting that, at these high protein/RNA ratios, some dimeric binding of the protein is occurring. In support of this is the fact that trans-binding experiments with RBD1L and LRBD2 also show an increase in polarization in this concentration range (data not shown). Removal of data points for protein concentrations above 100 μM nucleolin RBD12 from the curve and refitting them results in a K_D of 240 ± 30 nM with a better overall fit of the data (R^2 > 99%) (Figure 5C).

DISCUSSION

Linker Residues Connecting RBD1 and RBD2 Contribute to Affinity and Specificity of the Nucleolin RBD12/NRE Interaction. The role of the RBDs in nucleolin RBD12/NRE binding has previously been illustrated biochemically and genetically. These studies showed that mutation of several residues in the RBDs, especially those in the RNP motifs, abolishes or drastically decreases binding (*28*, *37*). Although binding to the NREs is not detectable for the individual RBDs, the attachment of the linker to the RBDs results in a weak, but specific, binding that is only detectable using equilibrium binding assays such as FA and NMR. The fact that no binding was observed for the RBDs without the linkers attached is probably explained by the numerous contacts between the linker and the RNAs in the nucleolin RBD12/sNRE and RBD12/b2NRE complex structures. One of the key features of the RBD12/NRE interaction is the insertion of the K94 side chain into the hole formed in both sNRE and b2NRE loops. The side chain of K94 is stacked on A14, and its ϵ-amino group likely hydrogen bonds to C11. Other linker residues that are important for RNA binding in the RBD12/sNRE and RBD12/b2NRE complexes are K89, which is in hydrophobic contact with C12; R91, which is hydrogen-bonded to G13; and K95, which makes nonspecific contacts to the RNA backbone. The data presented here, along with previous gel shift assays that showed that the

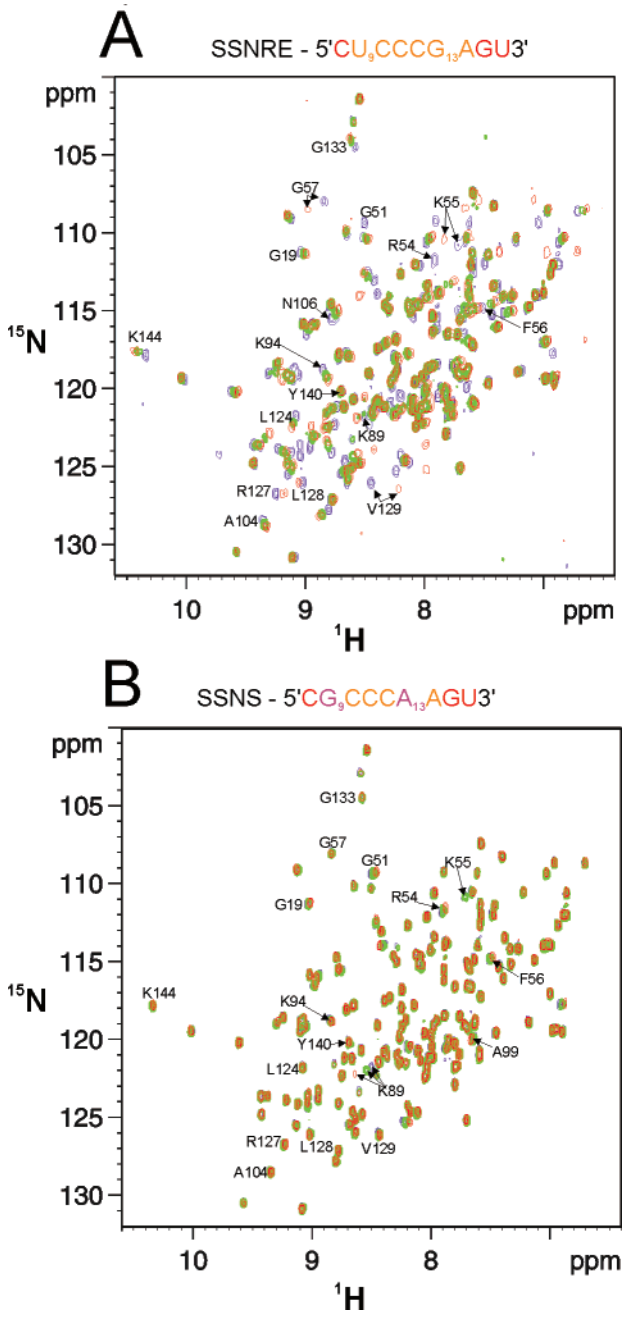

FIGURE 4: Nucleolin RBD12 sequence-specifically binds single-stranded NREs. (A) 600 MHz ^{1}H-^{15}N HSQCs of 0.15 mM ^{15}N-labeled nucleolin RBD12 free (purple), in a 1:0.5 complex (green) and in a 1:2 complex (red) with SSNRE. The sequence of SSNRE corresponds to nts 8−16 in b2NRE and is shown above the spectra with the NRE consensus colored orange and nonconsensus nucleotides colored red. (B) ^{1}H-^{15}N HSQCs of ^{15}N-labeled nucleolin RBD12 free (purple) in a 1:0.5 complex (green) and in a 1:2 complex (red) with SSNS. The sequence of b2ssNS is shown above the spectra with the same color scheme as in A. Mutations are shown in purple. Peaks that are labeled are those that are involved in the binding of the nucleolin RBD12/b2NRE complex (*31*).

mutation of K94 abolishes binding and the mutation of K89 and K95 results in weaker binding (*43*), indicate that the linker contributes to both affinity and specificity of the nucleolin RBD12/NRE interaction.

The weak binding of individual RBD1L and LRBD2 to sNRE and b2NRE was confirmed by NMR to be specific and likely similar to that observed in the structures of the nucleolin RBD12/sNRE and RBD12/b2NRE complexes. The

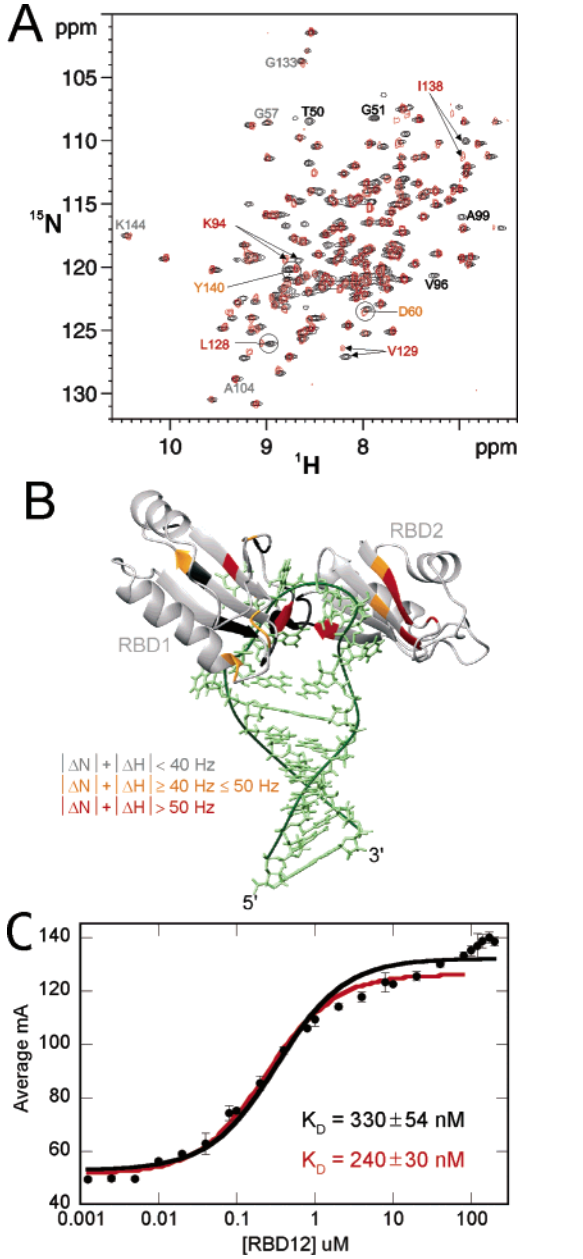

FIGURE 5: Comparison of nucleolin RBD12 in complex with b2NRE and SSNRE. (A) 600 MHz ^{1}H-^{15}N HSQC spectra of nucleolin RBD12 in a 1:1 complex with b2NRE (black) and in a 1:2 complex with SSNRE (red). Some of the amino acid residues are labeled. Grey, orange, and red labels indicate no or a very small chemical-shift difference ($|\Delta N| + |\Delta H| < 40$ Hz), moderate chemical-shift differences ($|\Delta N| + |\Delta H| > 40 \leq 50$ Hz), and large chemical-shift differences ($|\Delta N| + |\Delta H| > 50$ Hz), respectively. Black labels indicate that the amide signal disappears upon complex formation because of the binding kinetics in the intermediate exchange regime on the NMR time scale. (B) Chemical-shift differences observed in A illustrated on the lowest energy structure of the nucleolin RBD12/b2NRE complex (PDB accession code 1RJK) (*31*). The color scheme is the same as in A. (C) Binding isotherm of nucleolin RBD12 with SSNRE showing that the affinity for the single-stranded NRE is similar to the reported affinity of nucleolin RBD12/b2NRE (*29*). The binding isotherm was generated with 2 nM SSNRE and varying concentrations of nucleolin RBD12 (●). Each point is the average of five measurements, and the error bars reflect the standard deviation of those measurements. Data were fit to eq 2, and the resulting curve for all data points is represented by a black line, while the fit of the data to all points excluding those ≥100 μM is shown in red. The R^2 values for both fits are greater than 98%. The K_D's for nucleolin RBD12/SSNRE are shown.

relative affinities of the nucleolin RBD12 subdomain complexes studied are RBD1L/sNRE ≈ LRBD2/sNRE > LRBD2/b2NRE > RBD1L/b2NRE. A comparison of the structures of the nucleolin RBD12/sNRE and RBD12/b2NRE complexes explains the slightly greater affinity of the individual RBDs with the linker for sNRE compared to those for b2NRE. In the two complexes, the RBDs and linker make almost identical contacts to the NRE consensus nucleotides; however, in the nucleolin RBD12/sNRE complex, RBD1 and the linker also contact nonconsensus nucleotides in the upper portion of the loop E motif and A8, which stacks on the *trans*-Hoogsteen A•A base pair in the loop E motif (*36*, *43*). These additional contacts from the RBD1 and linker are likely responsible for the greater affinity of RBD1L and LRBD2 for sNRE compared to that for b2NRE. RBD1L and LRBD2 bind sNRE with affinities that are within the error of one another. This is consistent with the structure of the nucleolin RBD12/sNRE complex (*43*) because RBD1L and LRBD2 each contact seven nucleotides (Figure 3E). The lower affinity of RBD1L for b2NRE compared to LRBD2 is also consistent with the nucleolin RBD12/b2NRE complex structure, in which LRBD2 contacts six nucleotides, while RBD1L contacts four nucleotides.

Linker Is Necessary for the Cooperative Binding of Nucleolin RBD12 to NREs. NMR binding assays show that there is no trans binding even when one of the RBDs has the linker attached. Analysis of the nucleolin RBD12/sNRE and RBD12/b2NRE complexes indicates that the two RBDs and the linker make only a few interdomain contacts, which is consistent with the lack of trans binding. How then can the very weak affinities of the individual RBDs with the linker attached result in the nanomolar affinity for sNRE and b2NRE that is observed for a construct containing the RBDs in a cis arrangement? Biochemical studies of other tandem RBD proteins such as hnRNP A1 (*18*) and ASF/SF2 (*17*) have also shown that the individual RBDs maintain the ability to bind the RNA target, albeit with a decreased affinity (*14*, *17*, *18*). However, these studies did not address the role of the linker in binding specificity and affinity. Like the nucleolin RBD12/NRE interaction, analysis of binding affinities of the individual RBDs of ASF/SF2 and hnRNP A1 proteins shows that the affinity for the RNA target of the two RBDs in a cis arrangement is not simply the sum of the affinities of each individual RBD (*18*). The fact that the free energy of binding of isolated RBDs cannot simply be added to result in the affinity observed for the cis constructs of two RBDs can be attributed to the covalent attachment of the two RBDs by the linker. Covalent attachment of two small molecule ligands that bind a single protein at two separate sites is known to increase the affinity for the protein target because binding of the first ligand or domain increases the effective concentration of the second (*47*, *48*). This increase in binding affinity from cooperative binding through covalent linkage or dimerization [also known as the "chelating effect" (reviewed in ref *47*)] has been analyzed in detail for a variety of protein−DNA and protein−RNA complexes, including helix-turn-helix domains (*49*), Zn^{2+}-finger proteins (*50*−*53*), nuclear receptors (*54*), POU domains (*55*), bZip proteins (*56*), and RBDs (*9*). The cooperative binding behavior of covalently linked RBDs was predicted to increase the affinity for an RNA target 10- to 1000-fold compared to the affinity of the individual RBDs added together (*9*). Assuming no linker contacts to a RNA target and that the linker is a random coil with a interresidue distance of 3.5 Å, linkers longer than 60 amino acid residues are predicted to have a negligible effect on affinity, while linkers with less than 60 residues are predicted to gradually increase the affinity for an RNA target as the length of the linker is decreased (*9*). On the basis of this analysis and the fact that the linker in RBD12 is comprised of 12 amino acid residues, the increase in affinity because of a cis arrangement of the RBD1, linker, and RBD2 should be approximately 2 orders of magnitude greater than the simple addition of the binding affinities of the individual domains. However, the actual difference in affinity for b2NRE and sNRE caused by a cis arrangement of RBD1, linker, and RBD2 is 1000- and 100 000-fold, respectively. The 100-fold difference in the increase of affinity between b2NRE and sNRE with a cis arrangement of the domains is simply explained by the additional contacts from the linker and RBD1 to the loop E motif of sNRE as discussed above. The 10- and 1000-fold difference between the predicted and actual increase in affinity with a cis arrangement of RBD1, linker, and RBD2 for b2NRE and sNRE, respectively, is partially explained by the fact that the linkers in both complexes contact the NREs and are not in extended conformations, which were two of the basic assumptions of the theoretical study (*9*). Instead, the linkers in both NRE complexes line the major groove of the RNA loops and contain 3_{10} helices. The linker length between RBD1 and RBD2 (K89−T101) is 17.2 Å and 20.9 Å in the RBD12/sNRE and RBD12/b2NRE complexes, respectively, which is approximately half the predicted length for the 12 amino acid residue linker in an extended random-coil configuration (43.5 Å). Therefore, the contribution of the chelating effect to the affinity of the nucleolin RBD12/NRE complexes should be greater than predicted based on the number of linker residues alone. In addition, if the linker length between domains is considered to be the last linker/RNA contact to the second RBD, then the chelating effect will be even greater. Calculations that use linker lengths measured from the last linker/RNA contact to each RBD and the K_D's shown in Figure 2 (*9*) can fully account for the 10-fold difference between the predicted and the actual increase in affinity because of the chelating effect for the nucleolin RBD12/b2NRE interaction. On the other hand, similar calculations for the sNRE complex do not fully account for the 1000-fold difference between the theoretical and actual increase in affinity because of the chelating effect. This suggests that the nucleolin RBD12/sNRE interaction is also enhanced by other factors in addition to the chelating effect. One possibility is that conformational changes induced in sNRE by one RBD may positively affect the binding of the other covalently attached RBD (*47*). Another possibility is that binding of nucleolin RBD12 to sNRE may stabilize the adenine zipper that is only found in the lower portion of the RNA loop when the protein is bound (*29*, *30*).

Importance of a Stem-Loop Structure for Nucleolin RBD12/NRE Binding. Previous studies indicated that the higher stability of the nucleolin RBD12/sNRE complex compared to the nucleolin RBD12/b2NRE complex is due to the additional contacts from the RBD1 and linker to nucleotides outside the NRE consensus sequence in the nucleolin RBD12/sNRE complex (*31*). The presence of the S-shaped backbone in the loop E motif and the adenine

zipper-motif in sNRE provides a scaffold to which RBD1 and the linker make nucleotide-specific contacts. These contacts are not only dependent on the nucleotide identity, but also on the secondary structure context in which they are presented to the protein. In contrast to the complex with sNRE, the nucleolin RBD12/b2NRE complex showed that intermolecular contacts to the natural sequence are localized to the NRE loop consensus sequence. Therefore, binding of a single-stranded NRE to nucleolin RBD12 was investigated, as well. The NMR titrations show that the interaction of nucleolin RBD12 with SSNRE is specific, and the observed chemical-shift changes suggest that the contacts between nucleolin RBD12 and SSNRE are similar to those in the nucleolin RBD12/b2NRE complex. However, some residues in RBD2 and the linker in the nucleolin RBD12/SSNRE complex have chemical shifts that are different compared to both the free RBD12 and nucleolin RBD12/b2NRE complex, suggesting that these residues have unique chemical environments when nucleolin RBD12 is bound to a single-stranded NRE. Whether RBD1 residues in the nucleolin RBD12/SSNRE complex are in the same or different conformations in comparison to the nucleolin RBD12/b2NRE complex cannot be determined with the existing data because many of the amide resonances in RBD1 are broadened to baseline upon addition of SSNRE.

The largest chemical-shift differences between nucleolin RBD12 bound to SSNRE and b2NRE are displayed by I138 and K94. I138 is located in the RNP1 motif in RBD2 and packs closely against U9 in the nucleolin RBD12/b2NRE complex. The large chemical-shift difference of 110 Hz for this amide resonance may result from differences in contacts when bound to the SSNRE and/or in the RNA conformation. Because Y140 is not perturbed upon the addition of SSNRE as is the case for b2NRE and large chemical-shift differences are observed for I138 and residues in β2 of RBD2, it is likely that the 5′ end of SSNRE exits the β-sheet surface of RBD2 differently than the 5′ end of the b2NRE loop, which is constrained by the stem structure. The linker residue K94 inserts its side chain into the hole of the RNA loop in the RBD12/b2NRE complex. It is therefore not surprising that K94 displays a large chemical-shift difference in the complex with the single-stranded NRE versus a stem-loop NRE. The amide chemical-shift value of K94 is different from that in the free protein, indicating that K94 still interacts with the RNA in the SSNRE complex.

Upon titration of b2NRE and sNRE into nucleolin RBD12, almost all protein amides are in the slow-exchange regime on the NMR time scale (*31*), whereas the nucleolin RBD12/SSNRE titration displays fast/intermediate-exchange kinetics at the same field strength. The change from slow-exchange kinetics for the nucleolin RBD12/b2NRE complex to the fast/intermediate-exchange kinetics for the RBD12/SSNRE complex, even though FA assays at 4 °C show that the affinities are within the error of one another, could be caused by three factors. First, because chemical exchange behavior depends on the chemical-shift difference between the free and bound form, a smaller change in chemical shift could result in a change in the observed exchange regimes. However, some resonances in RBD2 have the same chemical shift in both the nucleolin RBD12/b2NRE and RBD12/SSNRE complexes (Figure 5A) and still display a change in the exchange regimes. Second, the on rate (k_{on}) and off rate (k_{off}) of the b2NRE and SSNRE complexes could both be different but could compensate for one another such that a difference in the K_D would not be observed. Third, the contradictory results from the NMR titrations and the FA assays may be due to the different temperatures at which the measurements were conducted. Unfortunately, FA assays on the nucleolin RBD12/NRE binding are suboptimal at higher temperatures (*29*). In summary, the interaction of nucleolin RBD12 with natural NREs such as b2NRE (300 nM) (*29*), which involves no stem contacts, does not require a stem-loop structure for binding. On the other hand, the low nanomolar binding (3 nM) of nucleolin RBD12 with sNRE is dependent on sequence-specific contacts to nonconsensus nucleotides at the bottom of the loop and in the loop E motif at the top of the stem.

Comparison to Other (RBD)$_2$/RNA Complexes. Like the nucleolin RBD12/sNRE and RBD12/b2NRE complexes, the linkers in the PABP/A_{11} (*38*), Sxl RBD12/U3−U11 (*39*), and HuD1,2/cfos-11 (*40*) complex structures also have 3_{10} helices and interact with the target RNA. In addition, the linkers are approximately the same length, with PABP, Sxl, and HuD having 10, 12, and 11 residues in their interdomain linkers, respectively. Because the RBDs of these proteins are covalently attached with relatively short linkers such as nucleolin RBD12, the chelating effect discussed above likely applies to these proteins as well. Furthermore, similar to the nucleolin RBD12 complexes, the linkers in the complexes discussed above also have lysine and/or arginine residues that contact the RNA targets via stacking, van der Waals, and/or specific hydrogen-bond interactions. Like the nucleolin RBD12/NRE complex, the secondary structure of the linker and the RNA contacts in these (RBD)$_2$/RNA complexes will result in an effective linker length shorter than predicted and, therefore, an even greater contribution of the chelating effect to the interaction. Thus, the linkers in several (RBD)$_2$/RNA complexes probably contribute to RNA binding in the same three ways as observed for the nucleolin RBD12/NRE interaction: affinity, specificity, and RBD cooperativity (chelating effect). In addition, the linkers between RBD23 and RBD34 in nucleolin are also short (21 and 14 amino acid residues, respectively) and contain positively charged amino acids (SWISS-PROT accession code P08199). Therefore, binding of RBD3, RBD4, and linker regions in nucleolin may contribute to the binding of other pre-rRNA sequences [e.g., the ECM (*23*, *26*)] in a manner similar to that seen for the nucleolin RBD12/NRE interaction.

Previous experiments using gel-shift or filter binding assays showed that a stem-loop structure was required for high-affinity binding of nucleolin RBD12 to the sNRE (1−5 nM) (*36*). Because other known (RBD)$_2$/RNA complexes such as PABP/(A_{11}) (*38*), Sxl RBD12/(U3−U11) (*39*), and HuD1,2/cfos-11 (*40*) have substrates that are single-stranded, the nucleolin RBD12/NRE interaction was thought to be unique because it was the only (RBD)$_2$/RNA interaction that required a stem-loop structure for binding. This requirement for a stem-loop structure is similar to that seen for the interaction of a single RBD to the U1A/U1 hairpin II (*57*). However, unlike the U1A/U1 hairpin II interaction, which absolutely requires a stem-loop structure to sequence-specifically bind its target sequence (*57*), nucleolin RBD12 can also bind sequence-specifically to single-stranded NREs with an affinity similar to that observed for the nucleolin

RBD12/b2NRE interaction (310 nM) (*29*). Therefore, nucleolin RBD12 is unique in that it is the only tandem RBD protein shown so far to be able to bind an RNA target sequence both as a single strand and in the context of a stem-loop structure, an observation that is consistent with the proposed chaperone function of the nucleolin/NRE interaction.

ACKNOWLEDGMENT

We thank Craig Blois for assistance with protein preparations, Dr. Carla Theimer for helpful discussion, Haihong Wu for critical reading of the manuscript, and Evan Feinstein for figure and manuscript preparation. The TEV S219N clone was a generous gift of the Doudna laboratory.

REFERENCES

1. Varani, G., and Nagai, K. (1998) RNA recognition by RNP proteins during RNA processing, *Annu. Rev. Biophys. Biomol. Struct. 27*, 407−445.
2. Burd, C. G., and Dreyfuss, G. (1994) Conserved structures and diversity of functions of RNA-binding proteins, *Science 265*, 615−621.
3. Ginisty, H., Sicard, H., Roger, B., and Bouvet, P. (1999) Structure and function of nucleolin, *J. Cell Sci. 112*, 761−772.
4. Bjork, P., Bauren, G., Jin, S. B., Tong, Y. G., Burglin, T. R., Hellman, U., and Wieslander, L. (2002) A novel conserved RNA-binding domain protein, RBD-1, is essential for ribosome biogenesis, *Mol. Biol. Cell 13*, 3683−3695.
5. Perez-Canadillas, J. M., and Varani, G. (2001) Recent advances in RNA-protein recognition, *Curr. Opin. Struct. Biol. 11*, 53−58.
6. Hall, K. B. (2002) RNA−protein interactions, *Curr. Opin. Struct. Biol. 12*, 283−288.
7. Birney, E., Kumar, S., and Krainer, A. R. (1993) Analysis of the RNA-recognition motif and RS and RGG domains: Conservation in metazoan pre-mRNA splicing factors, *Nucleic Acids Res. 21*, 5803−5816.
8. Ding, J. Z., Hayashi, M. K., Zhang, Y., Manche, L., Krainer, A. R., and Xu, R. M. (1999) Crystal structure of the two-RRM domain of hnRNP A1 (UP1) complexed with single-stranded telomeric DNA, *Genes Dev. 13*, 1102−1115.
9. Shamoo, Y., Abdulmanan, N., and Williams, K. R. (1995) Multiple RNA binding domains (RBDs) just don't add up, *Nucleic Acids Res. 23*, 725−728.
10. Scherly, D., Boelens, W., van Venrooij, W. J., Dathan, N. A., Hamm, J., and Mattaj, I. (1989) Identification of the RNA binding segment of human U1A and definition of its binding site on U1 snRNA, *EMBO J. 8*, 4163−4170.
11. Scherly, D., Boelens, W., Dathan, N. A., van Venrooij, W. J., and Mattaj, I. (1990) Major determinants of the specificity of interaction between small nuclear ribonucleoproteins U1A and U2B″ and their cognate RNAs, *Nature 345*, 502−506.
12. Hall, K. B., and Stump, W. T. (1992) Interaction of N-terminal of U1A protein with an RNA stem-loop, *Nucleic Acids Res. 20*, 4283−4290.
13. Kuhn, U., and Pieler, T. (1996) *Xenopus* poly(A) binding protein−Functional domains in RNA binding and protein−protein interaction, *J. Mol. Biol. 256*, 20−30.
14. Samuels, M., Deshpande, G., and Schedl, P. (1998) Activities of the sex-lethal protein in RNA binding and protein−protein interactions, *Nucleic Acids Res. 26*, 2625−2637.
15. Samuels, M. E., Bopp, D., Colvin, R. A., Roscigno, R. F., Garciablanco, M. A., and Schedl, P. (1994) RNA binding by Sxl proteins in vitro and in vivo, *Mol. Cell. Biol. 14*, 4975−4990.
16. Caceres, J. F., and Krainer, A. R. (1993) Functional Analysis of Premessenger RNA Splicing Factor Sf2/Asf Structural Domains, *EMBO J. 12*, 4715−4726.
17. Zuo, P., and Manley, J. L. (1993) Functional domains of the human splicing factor Asf/Sf2, *EMBO J. 12*, 4727−4737.
18. Shamoo, Y., Abdulmanan, N., Patten, A. M., Crawford, J. K., Pellegrini, M. C., and Williams, K. R. (1994) Both RNA-binding domains in heterogeneous nuclear ribonucleoprotein A1 contribute toward single-stranded-RNA binding, *Biochemistry 33*, 8272−8281.
19. Dreyfuss, G., Matunis, M. J., Pinolroma, S., and Burd, C. G. (1993) HnRNP proteins and the biogenesis of messenger RNA, *Annu. Rev. Biochem. 62*, 289−321.
20. Abe, R., Sakashita, E., Yamamoto, K., and Sakamoto, H. (1996) Two different RNA binding activities for the AU-rich element and the poly(A) sequence of the mouse neuronal protein MHuC, *Nucleic Acids Res. 24*, 4895−4901.
21. Park, S. M., Myszka, D. G., Yu, M., Littler, S. J., and Laird-Offringa, I. A. (2000) HuD RNA recognition motifs play distinct roles in the formation of a stable complex with AU-rich RNA, *Mol. Cell. Biol. 20*, 4765−4772.
22. Chung, S. M., Jiang, L., Cheng, S., and Furneaux, H. (1996) Purification and properties of HuD, a neuronal RNA-binding protein, *J. Biol. Chem. 271*, 11518−11524.
23. Ginisty, H., Amalric, F., and Bouvet, P. (2001) Two different combinations of RNA-binding domains determine the RNA binding specificity of nucleolin, *J. Biol. Chem. 276*, 14338−14343.
24. Srivastava, M., and Pollard, H. B. (1999) Molecular dissection of nucleolin's role in growth and cell proliferation: New insights, *FASEB J. 13*, 1911−1922.
25. Ghisolfi-Nieto, L., Joseph, G., Puvion-Dutilleul, F., Amaric, F., and Bouvet, P. (1996) Nucleolin is a sequence specific RNA-binding protein−Characterization of targets on pre-ribosomal RNA, *J. Mol. Biol. 260*, 34−53.
26. Ginisty, H., Serin, G., Ghisolfi-Nieto, L., Roger, B., Libante, V., Amalric, F., and Bouvet, P. (2000) Interaction of nucleolin with an evolutionarily conserved pre-ribosomal RNA sequence is required for the assembly of the primary processing complex, *J. Biol. Chem. 275*, 18845−18850.
27. Serin, G., Joseph, G., Faucher, C., Ghisolfi, L., Bouche, G., Amalric, F., and Bouvet, P. (1996) Localization of nucleolin binding sites on human and mouse pre-ribosomal RNA, *Biochimie 78*, 530−538.
28. Serin, G., Joseph, G., Ghisolfi, L., Bauzan, M., Erard, M., Amalric, F., and Bouvet, P. (1997) Two RNA-binding domains determine the RNA-binding specificity of nucleolin, *J. Biol. Chem. 272*, 13109−13116.
29. Finger, L. D., Trantirek, L., Johansson, C., and Feigon, J. (2003) Solution structures of stem-loop RNAs that bind to the two N-terminal RNA-binding domains of nucleolin, *Nucleic Acids Res. 31*, 6461−6472.
30. Allain, F. H.-T., Bouvet, P., Dieckmann, T., and Feigon, J. (2000) Molecular basis of sequence specific recognition of RNA stem-loops by nucleolin, *EMBO J. 19*, 6870−6881.
31. Johansson, C., Finger, L. D., Trantirek, L., Mueller, T. D., Kim, S., Laird-Offringa, I. A., and Feigon, J. (2004) Solution structure of the complex formed by the two N-terminal domains RNA-binding domains of nucleolin and a pre-rRNA target, *J. Mol. Biol. 337*, 799−816.
32. Wimberly, B., Varani, G., and Tinoco, I., Jr. (1993) The conformation of loop E of eukaryotic 5S ribosomal RNA, *Biochemistry 32*, 1078−1087.
33. Szewczak, A. A., and Moore, P. B. (1995) The sarcin/ricin loop, a modular RNA, *J. Mol. Biol. 247*, 81−98.
34. Correll, C. C., Freeborn, B., Moore, P. B., and Steitz, T. A. (1997) Metals, motifs, and recognition in the crystal structure of a 5S rRNA domain, *Cell 91*, 705−712.
35. Correll, C. C., Munishkin, A., Chan, Y. L., Ren, Z., Wool, I. G., and Steitz, T. A. (1998) Crystal structure of the ribosomal RNA domain essential for binding elongation factors, *Proc. Natl. Acad. Sci. U.S.A. 95*, 13436−13441.
36. Bouvet, P., Allain, F. H.-T., Finger, L. D., Dieckmann, T., and Feigon, J. (2001) Recognition of preformed and flexible elements of an RNA stem-loop by nucleolin, *J. Mol. Biol. 309*, 763−775.
37. Bouvet, P., Jain, C., Belasco, J. G., Amalric, F., and Erard, M. (1997) RNA recognition by the joint action of two nucleolin RNA-binding domains−Genetic analysis and structural modeling, *EMBO J. 16*, 5235−5246.
38. Deo, R. C., Bonanno, J. B., Sonenberg, N., and Burley, S. K. (1999) Recognition of polyadenylate RNA by the poly(A)-binding protein, *Cell 98*, 835−845.
39. Handa, N., Nureki, O., Kurimoto, K., Kim, I., Sakamoto, H., Shimura, Y., Muto, Y., and Yokoyama, S. (1999) Structural basis for recognition of the tra mRNA precursor by the sex-lethal protein, *Nature 398*, 579−585.

40. Wang, X. Q., and Hall, T. M. T. (2001) Structural basis for recognition of AU-rich element RNA by the HuD protein, *Nat. Struct. Biol. 8*, 141−145.
41. Dieckmann, T., and Feigon, J. (1997) Assignment methodology for larger oligonucleotides: application to an ATP-binding RNA aptamer, *J. Biomol. NMR 9*, 259−272.
42. Lucast, L. J., Batey, R. T., and Doudna, J. A. (2001) Large-scale purification of a stable form of recombinant tobacco etch virus protease, *BioTechniques 30*, 544−554.
43. Allain, F. H.-T., Gilbert, D. E., Bouvet, P., and Feigon, J. (2000) Solution structure of the two N-terminal RNA-binding domains of nucleolin and NMR study of the interaction with its RNA target, *J. Mol. Biol. 303*, 227−241.
44. Heyduk, T., Ma, Y., Tang, H., and Ebright, R. H. (1996) in *Methods Enzymol.* (Adhya, S., Abelson, J., and Simon, M., Eds.) pp 492−503, Academic Press, San Diego, CA.
45. Kay, L. E., Keifer, P., and Saarinen, T. (1992) Pure absorption gradient enhanced heteronuclear single quantum correlation spectroscopy with improved sensitivity, *J. Am. Chem. Soc. 114*, 10663−10665.
46. Sklenar, V., Piotto, M., Leppik, R., and Saudek, V. (1993) Gradient-tailored water suppression for ^{1}H-^{15}N HSQC experiments optimized to retain full sensitivity, *J. Magn. Reson., Ser. A 102*, 241−245.
47. Mammen, M., Choi, S. K., and Whitesides, G. M. (1998) Polyvalent interactions in biological systems−Implications for design and use of multivalent ligands and inhibitors, *Angew. Chem., Int. Ed. 37*, 2755−2794.
48. Crothers, D. M., and Metzger, H. (1972) The influence of polyvalency on the binding properties of antibodies, *Immunochemistry 9*, 341−357.
49. Robinson, C. R., and Sauer, R. T. (1996) Covalent attachment of Arc repressor subunits by a peptide linker enhances affinity for operator DNA, *Biochemistry 35*, 109−116.
50. Liu, Q., Segal, D. J., Ghiara, J. B., and Barbas, C. F. (1997) Design of polydactyl zinc-finger proteins for unique addressing within complex genomes, *Proc. Natl. Acad. Sci. U.S.A. 94*, 5525−5530.
51. Kim, J. S., and Pabo, C. O. (1998) Getting a handhold on DNA−Design of poly-zinc finger proteins with femtomolar dissociation constants, *Proc. Natl. Acad. Sci. U.S.A. 95*, 2812−2817.
52. Moore, M., Klug, A., and Choo, Y. (2001) Improved DNA binding specificity from polyzinc finger peptides by using strings of two-finger units, *Proc. Natl. Acad. Sci. U.S.A. 98*, 1437−1441.
53. Moore, M., Choo, Y., and Klug, A. (2001) Design of polyzinc finger peptides with structured linkers, *Proc. Natl. Acad. Sci. U.S.A. 98*, 1432−1436.
54. Ladias, J. A. A. (1994) Convergence of multiple nuclear receptor signaling pathways onto the long terminal repeat of human immunodeficiency virus-1, *J. Biol. Chem. 269*, 5944−5951.
55. Klemm, J. D., and Pabo, C. O. (1996) Oct-1 Pou domain DNA interactions−Cooperative binding of isolated subdomains and effects of covalent linkage, *Genes Dev. 10*, 27−36.
56. Morii, T., Saimei, Y., Okagami, M., Makino, K., and Sugiura, Y. (1997) Factors governing the sequence-selective DNA binding of geometrically constrained peptide dimers, *J. Am. Chem. Soc. 119*, 3649−3655.
57. Hall, K. B. (1994) Interaction of RNA hairpins with the human U1A N-terminal RNA binding domain, *Biochemistry 33*, 10076−10088.
58. Ginisty, H., Amalric, F., and Bouvet, P. (1998) Nucleolin functions in the first step of ribosomal RNA processing, *EMBO J. 17*, 1476−1486.
59. Hanakahi, L. A., Bu, Z. M., and Maizels, N. (2000) The C-terminal domain of nucleolin accelerates nucleic acid annealing, *Biochemistry 39*, 15493−15499.

BI049904D